

Lasers in Physics: Second-Harmonic Spectroscopy

J. I. Dadap and T. F. Heinz*

Department of Physics and Department of Electrical Engineering

Columbia University, 538 West 120th St.

New York, NY 10027

E-mail: tony.heinz@columbia.edu

Introduction

The demonstration of second-harmonic generation (SHG), one of the early experiments with pulsed lasers, is considered to have marked the birth of the field of nonlinear optics. The importance of second-harmonic generation, and the related phenomena of sum- and difference-frequency generation, as methods for producing new frequencies of coherent radiation was recognized immediately and has in no way diminished over the years. Associated with these applications came an interest in the fundamental nature of the second-order nonlinear response and some spectroscopic studies were undertaken with this motivation. This was a rather limited activity; it did not constitute a general method of optical probing of materials. In contrast, the third-order nonlinear optical interactions have given rise to a panoply of significant spectroscopic measurement techniques, including, to name a few, coherent Raman spectroscopy, pump-probe and other four-wave mixing measurements, two-photon absorption and hole burning measurements, photon echoes, and Doppler-free spectroscopy.

A central factor in the lack of spectroscopic applications of the second-order nonlinear response lies in a fundamental symmetry constraint. Unlike the third-order nonlinearity, which

is present in all materials, only materials lacking a center of inversion give rise to an (electric-dipole) allowed second-order nonlinear response. As we demonstrate in this article, however, it is just this property that makes SHG, as well as the sum-frequency generation process discussed elsewhere in this encyclopedia, such a remarkable probe of surfaces and interfaces. For centrosymmetric materials, the second-order nonlinear response is strong only at interfaces, where just a monolayer or so of material contributes to the response. This yields a purely optical probe (with incident and emitted photons) that gives an inherent surface sensitivity comparable to the best electron spectroscopies, such as electron-diffraction, Auger electron spectroscopy, photoemission spectroscopy, and scanning tunneling microscopy, the workhorses of surface science. Neither linear nor third-order nonlinear optical measurements provide this inherent interface sensitivity. The possibility of probing interfaces by purely optical means permits one to take advantage of several important features of optical radiation. Perhaps most noteworthy is the possibility of probing buried interfaces of every sort, from solid/solid to liquid/liquid, as well as the more conventional cases of solid/vapor, liquid/vapor, and liquid/solid. In addition, laser-based techniques offer unequalled capabilities for spectral or temporal resolution.

In this article, we present a brief overview of SH spectroscopy for the study of surfaces and interfaces. The article is divided into two principal sections: an introductory section that presents some of the fundamentals of SHG and the behavior at interfaces; and a discussion of the different types of information that the method can yield, as illustrated by some representative examples. A brief section on the experimental technique links these two parts.

Fundamentals of Surface SHG

Basic notions

Within the domain of classical optics, the response of a material to electromagnetic radiation is described by an induced polarization \mathbf{P} that varies linearly with the electric field strength, \mathbf{E} . This situation reflects the fact that strength of electric fields for light encountered under conventional conditions is minute compared to that of the electric fields binding atoms and solids together. The electric field binding an atom may estimated as $E_a \sim 1 \text{ V/\AA} = 10^{10} \text{ V/m}$. To reproduce this field strength by an electromagnetic wave requires an irradiance of $I_a \sim 10^{17} \text{ W/m}^2$, so the validity of this linear approximation in classical optics is well justified. The advent of the laser, with its capability for producing light beams with very high optical power and irradiance, has permitted us to probe and exploit the nonlinear response of materials, giving rise to the field of nonlinear optics.

The next-order material response beyond the linear approximation consists of an induced nonlinear source polarization $\mathbf{P}^{(2)} = \epsilon_0 \boldsymbol{\chi}^{(2)} : \mathbf{E}\mathbf{E}$ that depends quadratically on the driving electric field \mathbf{E} , described by a second-order nonlinear susceptibility $\boldsymbol{\chi}^{(2)}$. For excitation by a single laser at a frequency ω , this response gives rise to SHG at a frequency of 2ω , as well as optical rectification with a dc induced-polarization. For beams at two distinct frequencies of ω_1 and ω_2 , the processes of sum- or difference-frequency generation (SFG or DFG) become operative with the production of the new frequencies of $|\omega_1 \pm \omega_2|$. For a relationship of the given form, which assumes only a spatially local quadratic dependence of the polarization on the driving electric field, one can show that $\boldsymbol{\chi}^{(2)}$ must vanish within any centrosymmetric medium. This is a direct consequence of the fact that $\boldsymbol{\chi}^{(2)}$ as a quantity describing a centrosymmetric medium should not change under an inversion operation, while the quantities $\mathbf{P}^{(2)}$ and \mathbf{E} as polar vectors will change sign. The interface specificity of the SHG technique for centrosymmetric media follows from

this general observation: Only at interfaces is the bulk symmetry broken and the SHG process allowed.

Anharmonic oscillator model

Before we embark on our discussion of surface SHG, we first briefly consider a simple classical model of SHG based on an anharmonic oscillator. Although this is not a realistic treatment of the response of materials, it helps to illustrate the characteristic features of the surface SHG process and its spectroscopic attributes. In the anharmonic oscillator model, the medium is treated as a collection of electrons bound to fixed ion cores. While the usual Lorentz model only includes the effect of a linear restoring force, to describe second-order response, we generalize this description to include a leading-order anharmonic restoring force. For simplicity, we consider motion of the anharmonic oscillator in one spatial dimension, in which case the classical equation of motion for the displacement, x , of the electron can then be written as

$$\frac{d^2x}{dt^2} + 2\gamma\frac{dx}{dt} + \omega_0^2x - bx^2 = -\frac{e}{m}E(t). \quad (1)$$

Here $-e$ and m denote, respectively, the electron charge and mass, and $E(t)$ is the optical driving field. The (angular) frequency ω_0 defines the resonance of the harmonic component of the response, and γ represents a phenomenological damping rate for the oscillator. The nonlinear restoring force corresponds to the term containing the parameter b , a material-dependent constant. We are interested in the solution of this equation for a monochromatic driving field at frequency ω with amplitude $E(\omega)$ which we write as

$$E(t) = E(\omega)\exp(-i\omega t) + c.c., \quad (2)$$

An exact solution to Eq. (1) in the presence of this electric field is not possible. Let us, however, consider a regime in which we do not excite the oscillator too strongly, and the effect

of the anharmonic term remains relatively small compared to the harmonic one. In this case, we may solve the problem perturbatively in powers of the driving field. We find a linear response at the fundamental frequency and a nonlinear response at the SH frequency, which we can write in terms of the corresponding induced dipole moments $p = -e x$:

$$p(t) = p^{(1)}(\omega) \exp(-i\omega t) + p^{(2)}(2\omega) \exp(-i2\omega t) + c.c. \quad (3)$$

We can then write the amplitudes for the harmonically varying dipole moments as

$$p^{(1)}(\omega) = \alpha^{(1)}(\omega) E(\omega), \quad (4)$$

$$p^{(2)}(2\omega) = \alpha^{(2)}(2\omega = \omega + \omega) E(\omega) E(\omega), \quad (5)$$

where $\alpha^{(1)}$, the linear polarizability, and $\alpha^{(2)}$, the second-order polarizability (or first hyperpolarizability) for SHG are given, respectively, by

$$\alpha^{(1)}(\omega) = \frac{e^2}{m} \frac{1}{D(\omega)}, \quad (6)$$

$$\alpha^{(2)}(2\omega = \omega + \omega) = \frac{(e^3 / m^2) b}{D(2\omega) D^2(\omega)}. \quad (7)$$

Here we have introduced the resonant response at the fundamental frequency by $D(\omega) \equiv \omega_0^2 - \omega^2 - 2i\gamma\omega$, with a corresponding relation for the response $D(2\omega)$ at the SH frequency. A similar derivation can, of course, be applied to obtain the corresponding material response for the SFG or DFG processes.

The spectral dependence of the polarizabilities $\alpha^{(1)}$ and $\alpha^{(2)}$ are illustrated in Fig. 1 for the anharmonic oscillator model with a resonance frequency of ω_0 . In the linear case, one sees the expected behavior of the loss, associated with the $\text{Im}[\alpha^{(1)}]$, and dispersion associated with $\text{Re}[\alpha^{(1)}]$. A single resonance in the linear response is seen for the driving frequency ω near the oscillator frequency ω_0 . For the case of SHG, on the other hand, we observe both resonances

when the fundamental frequency $\omega \approx \omega_0$ and when the SH frequency $2\omega \approx \omega_0$. In quantum mechanical language introduced below, these peaks can be considered as arising, respectively, from matching of the fundamental and second-harmonic photon energies with the transition energy in the material.

In SHG spectroscopy, one normally measures the SH power as a function of the laser frequency. The SH field will scale with the nonlinear material response, *i.e.*, with $\alpha^{(2)}(2\omega=\omega+\omega)$, so that the SH power will be proportional to $|\alpha^{(2)}(2\omega=\omega+\omega)|^2$. Fig. 2 shows the corresponding spectra in the vicinity of the second-harmonic resonance. An important aspect of this type of spectroscopy, which is also present in other nonlinear spectroscopies, such as coherent Raman measurements, is the role that may be played by a non-resonant background. This may arise either from the off-resonant response of the system under study or from a coherent background from another material. In either case, the effect can be described by adding a spectral flat background response to the nonlinearity. Now when we detect the optical power, we then measure a quantity proportional to $|\alpha^{(2)}(2\omega=\omega+\omega)+k|^2$, where k represents the nonresonant background. The presence of k obviously elevates the baseline response near a resonance. In addition, however, depending on the relative phase of k , this extra term can introduce significant changes in the observed lineshapes. Fig. 2 illustrates this effect, which must always be borne in mind in the interpretation of experimental spectra.

For the purposes of studies of surfaces and interfaces, the key property of second-order nonlinear processes is the fact that they exhibit, for centrosymmetric bulk media, an inherent interface specificity. This feature can be readily understood in the context of the nonlinear oscillator model in which the SH polarization scales with the material parameter b . Since this term is associated with a potential that varies as x^3 , it is clear that the value of the b parameter

can be taken as a measure of the material's departure from inversion symmetry. At the interface, such a term can be present, reflecting the inherent asymmetry at a boundary, while it must necessarily be absent in the bulk of a centrosymmetric material.

Quantum-mechanical description of SHG

A correct description of SHG naturally requires a quantum mechanical treatment of the material response to the optical field. For our present purposes, we consider a localized entity with a nonlinear response, such as a non-centrosymmetric molecule at a surface. We consider below how these individual units can be added together to yield the surface nonlinear response of the material. Within this picture, we write the induced nonlinear dipole moment $\mathbf{p}^{(2)}$ of each molecule in terms of the driving electric field \mathbf{E} as

$$\mathbf{p}^{(2)}(2\omega) = \boldsymbol{\alpha}^{(2)}(2\omega=\omega+\omega):\mathbf{E}(\omega)\mathbf{E}(\omega). \quad (8)$$

This relation is simply the generalization of Eq. (5) to include a full 3-dimensional description, where $\mathbf{p}^{(2)}$ and \mathbf{E} are vectors and the second-order nonlinear polarizability $\boldsymbol{\alpha}^{(2)}$ is a third-rank tensor. The quantum mechanical description enters in how we relate the response function $\boldsymbol{\alpha}^{(2)}(2\omega=\omega+\omega)$ to the underlying properties of the material.

We can obtain an expression for the second-order nonlinear polarizability by application of second-order perturbation theory with the light-matter interaction treated as the perturbation. Within the electric-dipole approximation, the interaction Hamiltonian can be taken as $H_{\text{int}} = -\boldsymbol{\mu} \cdot \mathbf{E}(t)$, where $\boldsymbol{\mu} = -e\mathbf{r}$ denotes the electric-dipole operator and $\mathbf{E}(t)$ the electric field of the driving laser beam. Using the standard density-matrix formalism for second-order perturbation theory, one calculates for the Cartesian components $\alpha_{ijk}^{(2)}$ of the tensor $\boldsymbol{\alpha}^{(2)}$ as

$$\alpha_{ijk}^{(2)}(2\omega = \omega + \omega) = -\frac{1}{\hbar^2} \sum_{g,n,n'} \left[\frac{(\mu_i)_{gn}(\mu_j)_{nn'}(\mu_k)_{n'g}}{(2\omega - \omega_{ng} + i\Gamma_{ng})(\omega - \omega_{n'g} + i\Gamma_{n'g})} + \dots \right] \rho_g^{(0)}. \quad (9)$$

In this expression, the letters g , n' , and n represent energy eigenstates $|g\rangle$, $|n'\rangle$, and $|n\rangle$ of the system, with $\rho_g^{(0)}$ corresponding to the thermal population for differing available ground states g . As illustrated in Fig. 3, the SHG process can be regarded as involving a series of three transitions: two transitions associated with the absorption of two pump photons, each of energy $\hbar\omega$, and a transition associated with emission of a second-harmonic photon of energy $2\hbar\omega$. These transitions occur through the electric-dipole operator $\boldsymbol{\mu}$ and are characterized by the matrix elements $(\mu_i)_{gn}$. In Eq. (9), the energy denominators involve the energy differences $\hbar\omega_{ng} \equiv E_n - E_g$ and widths $\hbar\Gamma_{ng}$ for transitions between eigenstates $|n\rangle$ and $|g\rangle$, and similarly for other combinations of states. In addition to the term indicated explicitly in Eq. (9), there are several other very similar terms with different Cartesian coordinates in the matrix elements and/or frequency denominators.

The frequency denominators in the eight terms of Eq. (9) introduce a resonant enhancement in the nonlinearity when either the fundamental frequency ω or the SH frequency 2ω coincides with a transition from a ground state $|g\rangle$ to one of the intermediate states $|n'\rangle$ or $|n\rangle$. Fig. 3a shows the situation for a non-resonant nonlinear response, while Figs. 3b and 3c illustrate, respectively, single and two-photon resonances. The numerator in the perturbation theory expression consists of products of the three dipole matrix elements of the form $(\mu_i)_{gn}(\mu_j)_{nn'}(\mu_k)_{n'g}$. These terms reflect the structure and symmetry of the material that is built into the third-rank tensor $\alpha_{ijk}^{(2)}(2\omega = \omega + \omega)$.

The surface nonlinear response

As a model of the surface nonlinearity, let us consider a monolayer of oriented molecules. The surface nonlinear response accessible to a macroscopic measurement is given, under the neglect of local-field effects, simply by summing the response of the individual molecules. The resulting surface nonlinear susceptibility tensor $\chi_{s,ijk}^{(2)}$ connecting the induced nonlinear sheet polarization to the driving field electric field can then be expressed as

$$\chi_{s,ijk}^{(2)} = \frac{N_s}{\epsilon_0} \langle T_{i\lambda} T_{j\mu} T_{k\nu} \rangle \alpha_{\lambda\mu\nu}^{(2)}. \quad (10)$$

Here N_s denotes the adsorbate surface density, $\alpha_{\lambda\mu\nu}^{(2)}$ the nonlinear polarizability of the molecule expressed in its own coordinate system, $T_{i\lambda}$ the transformation tensor from the molecule's coordinate system to the laboratory frame, $\langle \rangle$ an ensemble average over the orientation of the different molecules in the monolayer, and $\epsilon_0 = 8.85 \times 10^{-12} \text{ F/m}$ the permittivity of free space. This expression for the surface nonlinear susceptibility has been successful in describing properties of adsorbed molecules, including their coverage, orientation, and spectroscopic features.

For the surfaces of materials such as semiconductors or metals with delocalized electronic states, a somewhat different formulation of the nonlinear response is appropriate. A modified version of Eq. (9) can be obtained using the relevant band states. The underlying concepts involved in the surface nonlinear response are, however, similar to those presented for the molecular case.

Regardless of the details of the model describing the surface nonlinear susceptibility, its tensor properties must reflect the symmetry of the interface. In that respect $\chi_{s,ijk}^{(2)}$ is quite

analogous to the bulk nonlinear response, $\chi_{ijk}^{(2)}$, in a non-centrosymmetric medium. In the absence of any symmetry constraints, $\chi_s^{(2)}$ will exhibit $3 \times 3 \times 3 = 27$ independent elements for SFG and DFG. For SHG, the order of the last two indices has no significance, and the number of independent elements is reduced to 18. If the surface exhibits a certain in-plane symmetry, then the form of $\chi_s^{(2)}$ will be simplified correspondingly. For the common situation of an isotropic surface, for example, SHG possesses 3 allowed elements of $\chi_s^{(2)}$ and may be denoted as $\chi_{s,\perp\perp\perp}^{(2)}$, $\chi_{s,\perp\parallel\parallel}^{(2)}$, $\chi_{s,\parallel\perp\perp}^{(2)} = \chi_{s,\parallel\parallel\perp}^{(2)}$, where \perp corresponds to the direction of the surface normal and \parallel to an in-plane direction. The nonvanishing elements of $\chi_s^{(2)}$ for other commonly encountered surface symmetries are summarized in several textbooks and reviews listed below.

Radiation properties for surface SHG

In order to probe and extract information from interfaces through surface SHG, it is necessary to understand how radiation interacts with the relevant media and gives rise to the experimentally observable signals. Here we present the principal results for the usual case of a spatially homogeneous planar interface. Non-planar and inhomogeneous geometries, which are also of considerable interest, will be considered briefly under the heading of applications of the SHG technique below.

The SHG process is coherent in nature. Thus, for the planar geometry, a pump beam impinging on the interface will give rise to a well-collimated SH radiation emerging in distinct reflected and transmitted directions. To describe this situation in a more detailed fashion and provide formulas for the radiation efficiency, we introduce a general description of SHG by a planar interface excited by a plane wave, as shown in Fig. 3. The nonlinear response of the

interface described by the surface nonlinear susceptibility tensor $\chi_s^{(2)}$ is incorporated through a nonlinear source polarization $\mathbf{P}^{(2)}$ of

$$\mathbf{P}^{(2)}(2\omega) = \mathbf{P}_s^{(2)}(2\omega)\delta(z) = \epsilon_0 \chi_s^{(2)}(2\omega = \omega + \omega) : \mathbf{E}(\omega)\mathbf{E}(\omega)\delta(z) \quad (11)$$

localized at the interface ($z = 0$). In addition to the strong nonlinear response at the interface, one must also generally consider the non-local nonlinear response of the bulk media. This response is much weaker than the symmetry-allowed interfacial response, but is permitted even in centrosymmetric materials. Since it is present in a much larger volume, however, its cumulative effect, while generally weaker than the surface response, may be of comparable magnitude. For simplicity, however, we neglect this constant background response in our discussion in this article, but a complete discussion can be found in the referenced works. The overall SH response is naturally also influenced by the linear optical properties of the surrounding media. The two bulk media and the interfacial region are characterized, respectively, by frequency-dependent dielectric functions ϵ_1 , ϵ_2 , and ϵ' , as shown in Fig. 3. Again for simplicity, and in accordance with most applications, we take the linear response to be isotropic.

Fig. 3 shows the incoming pump radiation and the reflected and transmitted SH beams. The directions of these beams are determined by conservation of the component of the momentum parallel to the interface in the SHG process, *i.e.*, $2\mathbf{k}_{\omega,\parallel} = \mathbf{k}_{2\omega,\parallel}^R = \mathbf{k}_{2\omega,\parallel}^T$. Thus the reflected and transmitted beams both remain in the plane of incidence, with directions governed by the so-called nonlinear Snell's law. For bulk media without dispersion between the frequencies of ω and 2ω the reflected and transmitted beams simply maintain the same angle of incidence as the pump beam. However, for dispersive bulk media, the directions of the beams are, however, altered, as can be understood immediately from writing $2k_\omega/k_{2\omega} = n_\omega/n_{2\omega}$, where

n denotes the refractive index of the medium. The surface SHG process does, nonetheless, differ in an important respect. In contrast to the situation for bulk media, the interfacial region is of negligible thickness, so phase shifts can obviously be disregarded. The issue of phase matching, which is of great significance for SHG from bulk media, consequently does not enter into the surface SHG problem.

By application of the Maxwell equations with the indicated nonlinear source polarization, one can derive explicit expressions for the SH radiation in terms of the linear and nonlinear response of the materials and the excitation conditions. For the case of the nonlinear reflection, the irradiance for the SH radiation can be written as

$$I(2\omega) = \frac{\omega^2 \sec^2 \theta |\mathbf{e}'(2\omega) \cdot \boldsymbol{\chi}_s^{(2)} : \mathbf{e}'(\omega) \mathbf{e}'(\omega)|^2 [I(\omega)]^2}{2\epsilon_0 c^3 [\epsilon_1(2\omega)]^{1/2} \epsilon_1(\omega)}, \quad (12)$$

where $I(\omega)$ denotes the irradiance of the pump beam at the fundamental frequency; c is the speed of light in vacuum; θ is the incidence angle of the pump beam. The vectors $\mathbf{e}'(\omega)$ and $\mathbf{e}'(2\omega)$ represent the polarization vectors $\hat{\mathbf{e}}_1(\omega)$, and $\hat{\mathbf{e}}_1(2\omega)$, respectively, after they have been adjusted to account for the linear propagation of the waves to the interface. More specifically, we may write $\mathbf{e}'(\omega) = \mathbf{F}_{1 \rightarrow 2} \hat{\mathbf{e}}_1(\omega)$. Here the $\mathbf{F}_{1 \rightarrow 2}$ describes the relationship between the electric field $E \hat{\mathbf{e}}_1$ in medium 1 (propagating towards medium 2), which yields a field $E \mathbf{e}'$ at the interface. For light incident in the x - z plane as shown in Fig. 3, $\mathbf{F}_{1 \rightarrow 2}$ is a diagonal matrix whose elements are $F_{1 \rightarrow 2}^{xx} = 2 \epsilon_1 k_{2,z} / (\epsilon_2 k_{1,z} + \epsilon_1 k_{2,z})$, $F_{1 \rightarrow 2}^{yy} = 2 k_{1,z} / (k_{1,z} + k_{2,z})$, and $F_{1 \rightarrow 2}^{zz} = 2 (\epsilon_1 \epsilon_2 / \epsilon') k_{1,z} / (\epsilon_2 k_{1,z} + \epsilon_1 k_{2,z})$, where the quantity $k_{i,z}$ denotes the magnitude of the z -component of the wavevector in medium i at the relevant wavelength (ω or 2ω).

A few observations may be made about Eq. (12), which describes the relationship between the typical experimental observables of the pump irradiance, $I(\omega)$, and the irradiance of the emitted SH reflection, $I(2\omega)$, from the interface. First, one can immediately recognize the quadratic relationship between the pump irradiance and the SH irradiance that is expected for a second-order nonlinear optical effect. Second, the SH radiation is determined not only by the nonlinear optical response, but by the linear optical properties of the relevant media. Consequently, obtaining the surface nonlinear susceptibility tensor $\chi_s^{(2)}$ from experiment requires knowledge or measurement of the linear response. (It should be noted, however, the interfacial linear properties always enter into the response in a fixed manner and can be incorporated into an effective surface nonlinear response.) The linear response can significantly enhance or reduce the efficiency of the SHG process. The use of a total-internal reflection geometry, for example, provides a significant enhancement in the SH radiation through the linear optical response of the media. Third, while full knowledge of the linear and nonlinear response will obviously allow one to predict the strength of the SH radiation for any conditions, a simple measurement of the SH response does not permit one to determine $\chi_s^{(2)}$, even if the linear optical properties are known. The determination of the tensor $\chi_s^{(2)}$ requires probing the material with different polarization states and/or angles of incidence. Protocols for making these measurements have been discussed extensively in the literature. For the general case of a material with in-plane anisotropy, such as the surface of a crystal, measurements of the response as the crystal is rotated about its surface normal are also very useful in a complete determination of $\chi_s^{(2)}$. Fourth, the simple measurement of the SH intensity as assumed here obviously eliminates information about the overall phase of the $\chi_s^{(2)}$. This phase information is often of considerable interest and

importance. For example, if the response of the interface is dominated by an oriented molecular monolayer, the sign of $\chi_s^{(2)}$ will be inverted if the monolayer is reflected through the plane of the surface, *i.e.*, the phase of $\chi_s^{(2)}$ yields information on the polar ordering of the layer. To obtain such phase information, one must employ a scheme using interference with a known SH reference. This approach, which is sketched briefly in the next section, is implemented quite commonly in experiment.

Experimental Considerations

The merits of the SHG technique for selective probing of interfaces are clear. On the other hand, one needs to be able to detect the optical signal associated with a second-order nonlinear response of a material that arises from an effective thickness of just a monolayer or so. Consequently, it is important to consider various factors that aid in optimizing the strength and detectability of the SH radiation. To discuss how best to achieve this end, let us recast Eq. (12) in terms of more convenient experimental parameters. We express the SH signal, S , in units of photons/s and describe the laser excitation by its pulse energy E_p , pulse width τ , and repetition rate R . For irradiation of an area A of the sample, we then obtain

$$S = \frac{\omega \sec^2 \theta E_p^2 R |\chi_{eff}^{(2)}|^2}{4\hbar \epsilon_0 c^3 \tau A}, \quad (13)$$

where $|\chi_{eff}^{(2)}|^2 \equiv |\mathbf{e}'(2\omega) \cdot \chi_s^{(2)} : \mathbf{e}'(\omega)\mathbf{e}'(\omega)|^2 / [\epsilon_1^{1/2}(2\omega)\epsilon_1(\omega)]$, whose typical value is of the order of $10^{-21} \text{m}^2/\text{V}$. From this relation, we see that increasing either the pulse energy or repetition rate of the laser will enhance our SH count rate. These parameters are, however, often limited by the characteristics of the available laser, as well as possible damage of the sample. For a given pulse energy and repetition rate, the SH signal is also seen to increase as the laser pulse duration or

sample area is decreased. In practice, adequate SH signals can generally be obtained from high power Q-switched lasers (with nanosecond pulses) with a fairly large focal spot. A preferred solution in most cases is, however, provided by modelocked lasers with high repetition rate and pulses of sub-picosecond duration. Surface SH signals obtained, for example, using a femtosecond modelocked Ti:sapphire oscillator, are typically in the range of 10^2 - 10^6 photons/s. Although these signals are relatively weak, they are easily detectable with photomultiplier tubes (PMT) and appropriate electronics.

The basic arrangement for surface SHG measurements is shown in Fig. 5. It makes use of the directionality and frequency selectivity of the SHG process not only to detect the desired signal with high efficiency, but to discriminate strongly against background signals, including the reflected laser beam. In the setup, irradiation of the sample involves a pulsed laser source, LS; a halfwave plate, λ , and polarizer, P, for controlling the input polarization. Spectral control is achieved with a filter F1 that passes the fundamental radiation in the pump beam, but rejects other wavelengths, particularly spurious SH radiation arising from other optical components; and a color filter F2 that passes SH, but rejects the reflected fundamental radiation. In addition, a spectrometer is commonly employed to limit the detection bandwidth further. An analyzer A serves to select the desired SH polarization. The SH signal is then measured by a high-quantum efficiency detector and the signal is monitored by processing electronics, typically a photon counter, a gated integrator, or a lock-in amplifier, depending on the strength of the signal and the repetition rate of the laser. The laser source may be either of fixed wavelength or tunable for spectroscopic measurements.

There are other important experimental configurations for surface SHG that extend beyond the basic SH reflection geometry, shown schematically in Fig. 6a. A common

improvement (Fig. 6b) is the implementation of a SH reference in which a small fraction of the pump radiation is directed into a crystal with a bulk second-order nonlinear response. This approach provides a reference against which to compare the measured signal that compensates appropriately for pulse-to-pulse variation in duration, energy, and spatial profile, as well as long-term drifts. This type of normalization (against a material with a suitably flat spectral response) is essential for spectroscopy measurements in which the laser frequency is scanned. In addition, use of a calibrated reference is the best way of determining the surface nonlinear response in absolute terms.

It may also be desirable to measure the *phase* of the signal. For this type of an experiment, a reference field, $\mathbf{E}_{\text{ref}}(2\omega)$, of similar amplitude and known phase response is generated along the path of the surface SH signal $\mathbf{E}(2\omega)$ (Fig. 6c). The two collinear SH beams of the same polarization interfere at the detector. The SH power scales as $|\mathbf{E}_{\text{ref}}(2\omega) + \mathbf{E}(2\omega)|^2 = |\mathbf{E}_{\text{ref}}|^2 + 2E_{\text{ref}}E \cos\varphi + |\mathbf{E}|^2$, where φ is the relative phase of the two fields. The relative phase φ may be varied by translating a reference plate along the path of the beam and making use of the dispersion of the ambient air or by inserting another control phase-shifting element. A variant of this phase measurement method is the homodyne scheme in which the reference electric field amplitude $\mathbf{E}_{\text{ref}}(2\omega)$ is significantly stronger than that of the signal amplitude $\mathbf{E}(2\omega)$. The measured SH power, then scales as $|\mathbf{E}_{\text{ref}}|^2 + 2E_{\text{ref}}E \cos\varphi$, which yields a signal that varies linearly with the desired SH field strength from the sample.

In the SHG technique, a short-pulse laser is used to interrogate the sample and thus the measurement provides high time-resolution. To make use of this capability, we can add a pump pulse to excite the sample away from equilibrium. This provides the opportunity to examine ultrafast surface dynamics induced by excitation of the sample with a suitable pump laser pulse.

For such measurements (Fig. 6d), the pump pulse is generally derived from the same laser source as the probe for the SHG measurement, although one or both of these pulses may undergo frequency conversion before being applied to the surface. The critical element is that time synchronism is maintained. The dynamics can then be followed by repeating the SHG measurement at various time delays relative to pump excitation, as controlled by an optical delay line. The ultimate time resolution of this technique is limited only by the duration of the laser pulses and may be as short as a few femtoseconds with state-of-the-art modelocked lasers.

Applications of Surface SHG

The technique of surface SHG is extremely flexible in application, since it relies only on basic symmetry properties for its remarkable surface or interface specificity. SHG measurements can provide quite varied information about the interface, depending on the mode of application of the technique and the material system under study. In this section, we attempt to illustrate the principal types of measurements that can be performed with SHG and the information that can be obtained thereby. For systems with molecular adsorbates, SHG studies can yield information on the density and orientation of molecular species, and can typically do so in real time. For crystalline surfaces, the symmetry and order of the surface can be examined through studies of tensor properties of the surface nonlinear susceptibility. Spectroscopic studies of electronic transitions are also of great value. These can be accomplished for both solids and molecular systems through the same experimental approach of tuning the frequency of the laser source. In all of these investigations, one can achieve very high time resolution, down into the femtosecond range, by the use of pump-probe techniques. In addition, as we discuss below, SHG provides

interesting additional capabilities for systems with applied electric and magnetic fields. Finally, the method permits one to probe spatially inhomogeneous systems.

In addition to this diverse range of information that can be provided by surface SHG measurements, the technique is unique in the extremely wide range of material and chemical systems to which it can be – and, indeed, has been – applied. These span the gamut from solids under ultrahigh vacuum to solid/solid, solid/liquid, liquid/vapor, and even liquid/liquid interfaces. Since our examples were drawn to illustrate the type of information obtainable, rather than the range of material systems investigated, the reader is unfortunately obliged to refer to other more detailed treatments of surface SHG measurements to appreciate fully this important facet of the technique.

Adsorbate density

The remarkably high sensitivity of the SHG technique to the nature of the surface is illustrated by the data in Fig. 7, which shows the dramatic change in the SH response from a clean Si(111)-7x7 surface upon adsorption of atomic hydrogen. Indeed, it is possible to detect well below 1% of a monolayer (ML) of adsorbed hydrogen. A useful point to note is that the change in $\chi_s^{(2)}$ is linear with adsorbate density for modest values of the coverage, θ . Thus, it is quite easy to obtain a relative gauge of the adsorbate coverage in this regime.

The behavior of the SH response to adsorbates at low coverages can often be described by a simple linearized model of the surface nonlinear susceptibility of $\chi_s^{(2)} = (1 - a\theta)\chi_{s,1}^{(2)} + \theta\chi_{s,2}^{(2)}$, where $\chi_{s,i}^{(2)}$ ($i = 1, 2$) are complex quantities and a is a constant. This relation describes the surface nonlinear susceptibility as arising from a contribution $\chi_{s,1}^{(2)}$ from the clean surface and a

contribution $\chi_{s,2}^{(2)}$ from a saturated monolayer ($\theta = 1$) of the adsorbate. The term $-a\theta\chi_{s,1}^{(2)}$ then represents the modification of the surface nonlinearity arising from interaction with the adsorbate. For the case of hydrogen adsorption of Fig. 7, this is the dominant term, since hydrogen *atoms* would have no nonlinearity on their own. In other systems, however, the response can be considered as arising essentially from the nonlinear response of aligned adsorbed molecules. The simple linearity of this relation of $\chi_s^{(2)}$ with adsorbate coverage obviously neglects important effects such as adsorbate-adsorbate chemical interactions, as well as local field effects and the possible influence of differing adsorption sites. All of these factors have been considered in the literature. Nonetheless, the linearity of response with adsorbate coverage is often found to be a good approximation, even for fairly high adsorbate coverages. From the point of view of simply following adsorption dynamics with SHG, it is not, we note, necessary to have any *a priori* knowledge of the relation between the adsorbate coverage and the SH response. This relation can be established empirically in static measurements and then used advantageously to follow the dynamics of surface processes.

Surface symmetry and molecular orientation

The surface SHG process is described by the third-rank tensor $\chi_s^{(2)}$. The tensorial properties of this response reflect the symmetry of the surface. Other than for a few cases of high symmetry, such a third-rank tensor gives a distinct signature of surfaces with crystalline order compared to surfaces, such as disordered ones, exhibiting effective in-plane isotropy. The form of the $\chi_s^{(2)}$ tensor can be probed both by measurements that vary the polarization of the fundamental and second-harmonic beams and by measurements in which the plane of incidence

is changed with respect to the orientation of the surface, generally by rotating the sample about its normal with a fixed experimental geometry.

Fig. 8 illustrates the capability of surface SHG measurements to probe surface symmetry. The figure shows SHG polarization dependence for a Si(111) surface cleaved in ultrahigh vacuum. While the underlying bulk symmetry suggests that the surface might exhibit $3m$ symmetry, the data clearly indicate that only a single mirror m plane is present. This lowered symmetry corresponds to the metastable 2×1 reconstruction induced by the crystal cleavage. By heating the sample, one can observe a phase transformation to the equilibrium 7×7 reconstruction and the emergence of the corresponding $3m$ surface symmetry.

The analysis of surface or interface symmetry by SHG relies only on the *form* of the nonlinear susceptibility tensor, *i.e.*, which elements are independent and nonvanishing. Within the context of a microscopic model of the surface response, however, the *relative values* of the tensor elements of $\chi_s^{(2)}$ can also yield valuable information about the nature of the surface. This approach has been developed extensively in the context of the analysis of molecular orientation at surfaces. The basic notion behind this treatment relies on the knowledge of the microscopic molecular nonlinear polarizability $\alpha_{\lambda\mu\nu}^{(2)}$ and the measured surface nonlinear susceptibility $\chi_{s,ijk}^{(2)}$ to infer information about the orientational average that relates these quantities. As discussed above in conjunction with Eq. (10), under the neglect of local-field corrections, the relationship between these two quantities involves the ensemble average of the coordinate transformation tensor from the molecular to the laboratory coordinate systems $\langle T_{i\lambda} T_{j\mu} T_{kv} \rangle$. Hence a knowledge of the quantities $\alpha_{\lambda\mu\nu}^{(2)}$, N_s , and $\chi_{s,ijk}^{(2)}$ allows us to infer information about the orientational distribution of the molecules as described by the quantity $\langle T_{i\lambda} T_{j\mu} T_{kv} \rangle$. Even in the absence of

knowledge of the magnitudes of the nonlinear polarizabilities and the adsorbate density, one may still obtain useful information for molecules with a simple form of $\alpha_{\lambda\mu\nu}^{(2)}$.

An important example of this analysis of molecular orientation concerns the case of molecules with a dominant nonlinear polarizability along a single axis, *i.e.*, $\alpha^{(2)} = \alpha_{z'z'z'}^{(2)} \hat{\mathbf{z}}'\hat{\mathbf{z}}'\hat{\mathbf{z}}'$. For the usual situation of in-plane isotropy, one can then show that the nonlinear susceptibility elements are given by $\chi_{s,\perp\perp\perp}^{(2)} = N_s \langle \cos^3 \theta \rangle \alpha_{z'z'z'}^{(2)} / \epsilon_0$ and $\chi_{s,\parallel\perp\perp}^{(2)} = \chi_{s,\parallel\parallel\perp}^{(2)} = \frac{1}{2} N_s \langle \cos \theta \sin^2 \theta \rangle \alpha_{z'z'z'}^{(2)} / \epsilon_0$, where θ denotes the angle between the surface normal and the z' molecular axis. It should be noted that these orientational moments, reflecting their origin in a third-rank tensor, give a signature of the polar ordering, since a sign change in the elements of $\chi_s^{(2)}$ follows if the molecular orientation is inverted. Also, when only one element of $\alpha^{(2)}$ is present, we can form ratios of the experimentally measurable ratio of tensor elements that depend only on the molecular orientational factors, such as $R \equiv (2\chi_{s,\parallel\perp\perp}^{(2)} + \chi_{s,\perp\perp\perp}^{(2)}) / \chi_{s,\perp\perp\perp}^{(2)} = \langle \cos \theta \rangle / \langle \cos^3 \theta \rangle$. For a narrow distribution of the orientations centered at θ_0 , this ratio yields directly the molecular orientation angle through $R \approx \sec^2 \theta_0$.

This type of molecular orientation analysis has been applied to a wide range of material systems. The method, while powerful, relies on several assumptions, including an adequate knowledge of the molecular nonlinear polarizability, the lack of significant local field corrections, the availability of information about the effective linear dielectric constant in the interfacial region, and a suitable method of eliminating any substrate nonlinear response in the measurement. The method is, consequently, best suited for adsorbed layer of molecules with strong and well-defined nonlinear response, present at relatively modest coverages. The use of resonant excitation is a valuable adjunct in these studies, since it generally simplifies the form

and strengthens the molecular nonlinear response. An analogous approach to the analysis of molecular orientation can be accomplished with infrared-visible sum-frequency generation. These measurements often provide a superior method of analysis, since the molecular response and its symmetry are better defined by resonant excitation of a molecular vibration.

Surface and interface spectroscopy

Surface SHG can be readily adapted to yield spectroscopic information on surface transitions. As indicated above, both resonances at the fundamental and second-harmonic frequencies are manifested in the SHG response. The examination of resonances at the SH frequency is often convenient, since it permits the application of a relatively intense pump radiation at a frequency well separated from that of the resonance. Such SHG spectroscopy measurements have been widely applied to examine electronic transitions at surfaces and interfaces of solids, as well as in adsorbed molecules under a wide variety of conditions.

An example of SHG spectroscopy of electronic transitions at a buried solid/solid interface is presented in Fig. 9. For the epitaxial $\text{CaF}_2/\text{Si}(111)$ interface, distinctive new electronic transitions, associated with interface states, are observed that are absent from the response of either of the bulk materials. These excitations occur in a spectral range where the bulk silicon sample is highly absorbing, which would render the identification of the new interface transitions very difficult using conventional linear optics. The buried nature of the interface naturally also constrains application of conventional surface probing techniques involving electron irradiation or emission. Two additional general observations are appropriate. First, the lineshape analysis for such measurements must take into account the fact that the SHG response derives from both the real and imaginary parts of $\chi_s^{(2)}$, as we discussed above. Second, in the absence of any other

knowledge, SHG spectroscopic data contain an ambiguity about whether the resonances correspond to the fundamental or SH photon energy. This ambiguity, however, can be resolved in a straightforward fashion by complementing the SHG measurement with a sum-frequency measurement in which one frequency is scanned and one is held fixed, as was demonstrated in the study associated with Fig. 9.

Time-resolved measurements

One of the fascinating frontiers that can be addressed by SHG measurements is probing the ultrafast dynamics of surfaces and interfaces by the pump-probe method. This possibility is exemplified by a variety of studies ranging from the dynamics of laser-driven phase transitions, charge-transfer, solvation, phonon dynamics, and orientational and torsional dynamics.

An example of applying time-resolved SHG to examine ultrafast molecular dynamics at the liquid/vapor interface of water is presented in Fig. 10. In these studies, the rotational motion of dye molecules at the interface, which probes the local environment, is followed in real time. This is accomplished by photo-exciting the dye molecules at the interface. Because polarized pump radiation is used, an anisotropic orientational distribution of excited-state molecules is established. Since the excited molecules have a different SHG response, a change in the signal is observed immediately. Subsequently, the anisotropic orientational distribution relaxes to the equilibrium configuration. The time evolution of the rotational anisotropy is followed by detecting the SH of a probe laser pulse as a function of the delay time. Through a comparison of the results for different initial anisotropic distributions (produced by pump beams with differing polarizations), one may deduce rates for both in-plane and out-of-plane orientational relaxation.

This example illustrates the possibilities of time-resolved SHG measurements for probing the detailed dynamics of molecules at an interface on the ultrafast time scale.

Spatially-resolved measurements

Up to this point, our discussions have centered on spatially homogenous surfaces and interfaces. Surface SHG has also been exploited to probe the lateral variation of inhomogeneous surfaces with the micron to sub-micron resolution characteristic of optical microscopy techniques. Spatial resolution may be achieved simply by detecting the nonlinear response with a focused laser beam that is scanned across the surface. A large area of the surface may also be illuminated and the emitted nonlinear radiation imaged. A wide range of applications of this imaging capability has emerged, including the probing of biological materials, such as cells and tissues, to probing spatially varying electric fields and magnetic domains. Within the biological context, SH microscopy has recently become an active research direction. In these applications, while probing with SHG typically senses non-centrosymmetric structures in bulk samples as opposed to interfaces, most of the aspects of SHG presented in this article still apply. To further improve the spatial resolution of SHG microscopy, researchers have also employed near-field techniques for spatial resolutions below the diffraction limit.

Complementary approaches to the real-space imaging just described have also been developed based on SH diffraction. In this scheme, periodically modulated surfaces are established holographically on a surface by utilizing two interfering laser beams. In addition to the reflected and transmitted SH beams, additional beams are then generated at well-defined angles as dictated by the grating period. This approach has been used to monitor the relaxation of

a monolayer grating of adsorbates in time, which yields precise information on the rate of adsorbate surface diffusion.

Probing electric fields at interfaces

For centrosymmetric media, the SHG process shows a high degree of sensitivity to the presence of electric fields. This property follows from the fact that an applied electric field can break the inversion symmetry, just as an interface does. The resulting process, termed electric field-induced SHG (or EFISH), has been known for many years. From a phenomenological standpoint, it can usually be described as a nonlinear response of the form $\mathbf{P}^{(3)}(2\omega) = \epsilon_0 \chi^{(3)} : \mathbf{E}(\omega) \mathbf{E}(\omega) \mathbf{E}$, where \mathbf{E} is the electric-field being probed and $\mathbf{E}(\omega)$ is the laser pump field. Within the context of surfaces and interfaces, there are many circumstances where probing such electric fields is of interest and importance. The SHG technique provides high sensitivity, good spatial resolution, accessibility to buried interfaces, and, in the pump-probe implementation, extremely high time resolution. In addition, with appropriate measurements of the polarization dependence and homodyne detection, the full vector character of the electric field can be determined.

The behavior of electric-field induced SHG is similar to that arising from the asymmetry of an interface. Indeed, it is formally equivalent to the response of an interface provided that the electric field is present in (or radiates from) a region of less than a wavelength's thickness. The applications of this measurement capability are quite diverse, ranging from studies of charging and acid/base reactions at liquid/solid interfaces to probing fields in metal-oxide-semiconductor structures and Schottky barriers to the measurement of freely-propagating terahertz radiation. In Fig. 11, SHG with appropriate polarization control and homodyne detection scheme has been

applied to the measurement of the vector character of electric fields present in a dc-biased dipole structure on silicon. By spatially scanning the laser beam, a two-dimensional electric field map can be produced. In a pump/probe scheme, the same measurements can be made with femtosecond time resolution.

Probing magnetization at interfaces

In contrast to the application of an external electric field (a polar vector), the presence of an external magnetic field (an axial vector) does not break the inversion symmetry of a material. Thus, SHG retains its interface selectivity for magnetic effects. SHG measurements, as an interface specific probe, thus provide an excellent complement to the linear magneto-optical Kerr effect (MOKE), which is sensitive to magnetic effects within the penetration depth of the light.

The ability of the SHG technique to sense the magnetization at a surface is illustrated in Fig. 12 for a film of epitaxially-grown magnetic Co on nonmagnetic substrate Cu. A hysteresis loop of the magnetization versus the strength of an applied magnetic field is shown, where the magnetization is gauged from the SHG response. Through measurements of the response as a function of the thickness of the magnetic film, the researchers demonstrated that the SH response reflected the interface properties, rather than those of the bulk film.

Probing micro- and nanoscale structures

In addition to the microscopy studies described above that probe spatially inhomogeneous surfaces, there has been considerable interest in SHG from a variety of strongly textured surfaces and small particles. From the standpoint of the optical response of materials, particular interest has been attached to studies of metallic surfaces with surface roughness. For

appropriate roughness of low-loss materials, such as silver, very significant local-field enhancements can be achieved. Since these field enhancements enter into the strength of the SH emission nonlinearly, overall enhancements in the SH power by several orders of magnitude have been demonstrated. This provides both a useful method of study of such surface enhancement effects and a scheme for amplifying the relatively weak surface nonlinear response.

Beyond these problems associated with roughened surfaces, considerable attention has recently been directed towards the application of the SHG technique for probing micro- and nano-scale particles. The fundamental principle of the interface selectivity of the SHG process for such systems comprised of centrosymmetric materials remains unaltered. The interaction of these particles with the radiation fields is, however, significantly modified. For the case of particles of with dimensions of several optical wavelengths, the overall SHG signal strength may be comparable to that from a corresponding area of a planar surface. The radiation pattern will, of course, be strongly modified and will generally be diffuse in character. While this makes detection (and background discrimination) somewhat more difficult than for the planar geometry, many SHG measurements of surface and interface properties have been carried out in this regime. As the particle size becomes progressively smaller, particles with overall inversion symmetry begin to exhibit appreciable cancellation of the SH emission. Indeed, in the limit of vanishing size, full cancellation is expected. This tendency is, however, offset by the increasing surface-to-bulk ratio and the possibility of increasing the number of particles probed. It has been demonstrated experimentally that the surfaces of particles in the nanometer length scale can indeed be probed by SHG.

From the point of view of applications, this extension of the SHG technique to probe micro- and nano-structured materials opens up a rich variety of new possibilities. Results have

been reported on metal and semiconductor nanoparticles in suspension, as well as on colloids of minerals. In addition, liquid droplets have been investigated. Self-assembling structures such as liposomes and vesicles have been examined. For these structures, many of the same capabilities of SHG as demonstrated for the planar geometry, such as probing of adsorption and charging effects, have been demonstrated. More uniquely, molecular transport *through* the liposome membrane could also be observed and characterized. The possibility of extension of these measurements to biological systems is of obvious interest and promise.

Concluding Remarks

In this article, we provided a brief review of surface SHG as a technique for interface-specific probing of materials. In addition to discussing some of the fundamental ideas underlying the method, we outlined the wide variety of information that may be obtained from such measurements, ranging from surface symmetry and molecular ordering to interface spectroscopy and ultrafast dynamics. While several aspects of the method have now become quite well established, developments in widely available modelocked lasers with excellent performance characteristics have greatly enhanced the ease of making surface SHG measurements in a wide class of material systems. In addition, new developments and applications of the method have continued to emerge apace. Of particular note in this regard are applications to probe electric fields and magnetization at interfaces, as well as advances in the use of the method for interface-specific probing of micro- and nanoscale structures. The sharp increase in applications of SHG for probing systems of biological importance constitutes another important development, and one with much promise for the future.

One of the authors (TFH) would like to acknowledge support for this work from the U.S. Department of Energy, Office of Basic Energy Sciences, through the Catalysis Science Program.

Figure Captions

1. Real and imaginary components of the linear polarizability $\alpha^{(1)}(\omega)$ (top panel) and the second-order nonlinear polarizability $\alpha^{(2)}(2\omega=\omega+\omega)$ (bottom panel) plotted versus frequency according for the anharmonic oscillator model. For the SH response, the resonance features at $\omega = \omega_0$ and $\omega = \omega_0/2$ correspond, respectively, to single-photon and two-photon resonances.
2. SH spectra $I(2\omega)$ versus pump laser frequency ω corresponding to Fig. 1 in the vicinity of the two-photon resonance, with and without the presence of a non-resonant (frequency-independent) background: $I(2\omega) \sim |\alpha^{(2)}(2\omega=\omega+\omega) + k|^2$, where k represents a constant background and parametrized through $k = m|\alpha^{(2)}(2\omega=\omega_0)|$ and m is constant factor. Top panel: $m = 0, 0.5, 1$ (bottom to top curves). Bottom panel: $m = 0, 0.5i, i$ (bottom to top curves). In the top panel, the upper two lineshapes were displaced vertically to distinguish the three curves.
3. Quantum mechanical description of SHG process for the situations of a) nonresonant, b) single-photon resonant, and c) two-photon resonant interactions. SHG occurs through transition from the initial state electronic state $|g\rangle$ and a first intermediate state $|n'\rangle$, then to a second intermediate state $|n\rangle$, followed by a return to the initial state. The process is just a parametric conversion of two photons at frequency ω into one photon at frequency 2ω .
4. Schematic representation of SHG at the interface between two centrosymmetric media. The pump field $\mathbf{E}(\omega)$ at frequency ω with corresponding wavevector \mathbf{k}_ω is incident on the interface from medium 1. The SH field $\mathbf{E}(2\omega)$ at frequency 2ω is emitted in directions described by the wavevectors $\mathbf{k}_{2\omega}^R$ (reflected in medium 1) and $\mathbf{k}_{2\omega}^T$ (transmitted in medium 2). The linear dielectric constants of media 1, 2, and the interface are denoted, respectively, by ϵ_1 , ϵ_2 , and ϵ' . The nonlinear response of the interface ($z=0$) is given by the surface nonlinear susceptibility tensor $\chi_s^{(2)}$.

5. Schematic representation of a basic surface experimental setup for surface SHG. It is comprised of laser source (LS), halfwave plate (λ), polarizer (P), lenses (L), spectral filters (F1, F2), analyzer (A), and detector (D).
6. Various schematic representations of different experimental schemes for surface SHG measurements. Panel (a) represents the basic scheme as in Fig. 5. Panel (b) describes use of separate SHG source as a reference for normalizing the surface SHG signals against laser fluctuation and drift. Panel (c) represents the arrangement for a measurement of the phase of the surface SHG signal by mixing the fields from the surface and an external source SH radiation. Panel (d) describes the configuration for a time-resolved measurement using the pump-probe scheme.
7. Dependence of the magnitude (full circles) and the phase (open squares) of the nonlinear susceptibility $\chi_s^{(2)}$ for a Si(111)-7 \times 7 surface as a function of the coverage of adsorbed atomic hydrogen using a fundamental photon energy 1.17 eV. (After U. Höfer, Appl. Phys. A **63**, 533 [1996].)
8. Polarization dependence of SHG for normal incidence excitation of the cleaved Si(111)-2 \times 1 surface. The polar plot of the SH signal versus the pump polarization orientation is shown for the case of no polarization analysis (top panel), for the SH analyzer along the $[2\bar{1}\bar{1}]$ crystallographic direction of the surface (middle panel), and along the $[0\bar{1}\bar{1}]$ direction (bottom panel). The solid curves are fits to theory assuming that the surface has m symmetry (After T. F. Heinz *et al.*, Phys. Rev. Lett. **54**, 63 [1985].)
9. SHG spectrum (solid dots) for the CaF₂/Si(111) interface. For comparison, the open circles represent the corresponding signals for the SiO₂/Si(111) interface, which is seen to give a very weak signal in this frequency range. The solid line is a theoretical fit based on a two-dimensional direct transition of the interface states, together with an excitonic feature slightly below the band gap. (After T. F. Heinz *et al.*, Phys. Rev. Lett. **63**, 644 [1989].)

10. Rotational relaxation of Coumarin 314 molecules at the air-water interface subsequent to photoexcitation. The initial anisotropy in the molecular orientational distribution is created by linearly-polarized pump radiation in two orthogonal directions in the surface. (After D. Zimdars *et al.*, *J. Phys. Chem. B* **103**, 3425 [1999].)

11. Vector map of the electric field in Si-on-sapphire substrate as deduced by SHG measurements. A voltage is imposed on the rectangular metallic electrodes, which are separated by 80 μm . (After J. I. Dadap *et al.*, *Opt. Lett.* **24** 1059 [1999].)

12. SH response of a Co film on a Cu(001) substrate as a function of the applied magnetic field. A hysteresis loop corresponding to the surface response is observed. (After H. A. Wierenga *et al.*, *Phys. Rev. Lett.* **74**, 1462 [1995].)

Fig. 1.

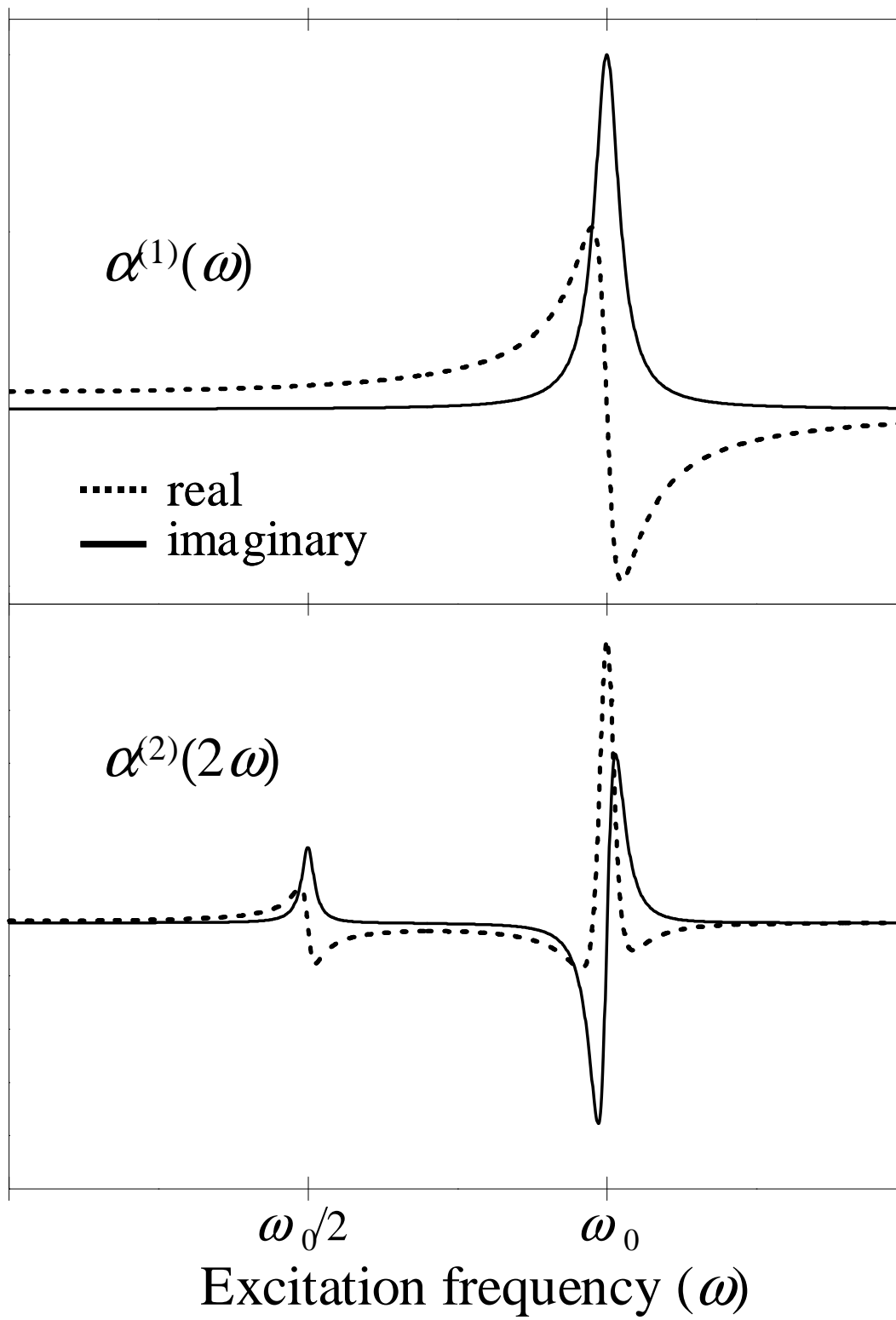


Fig. 2

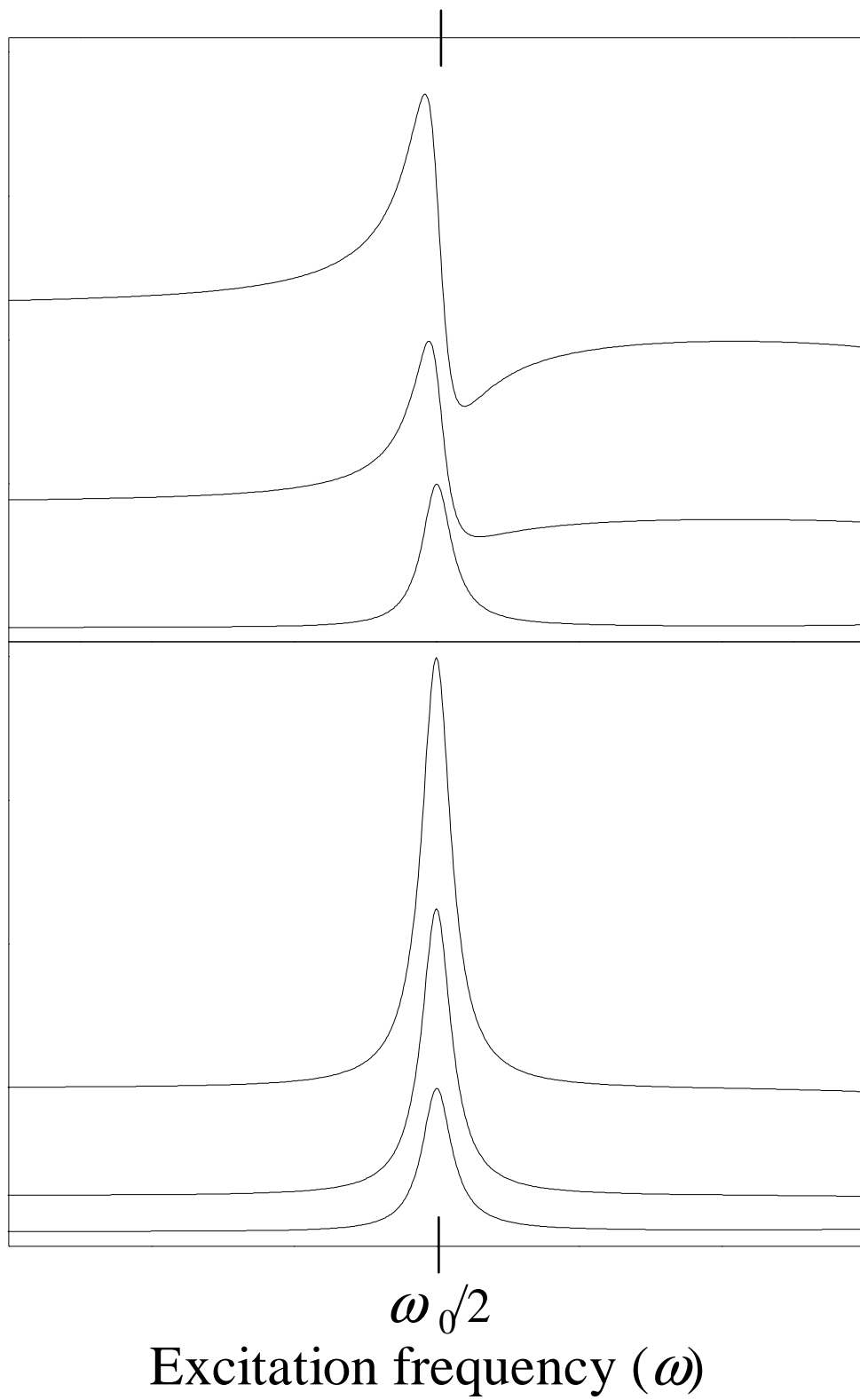


Fig. 3

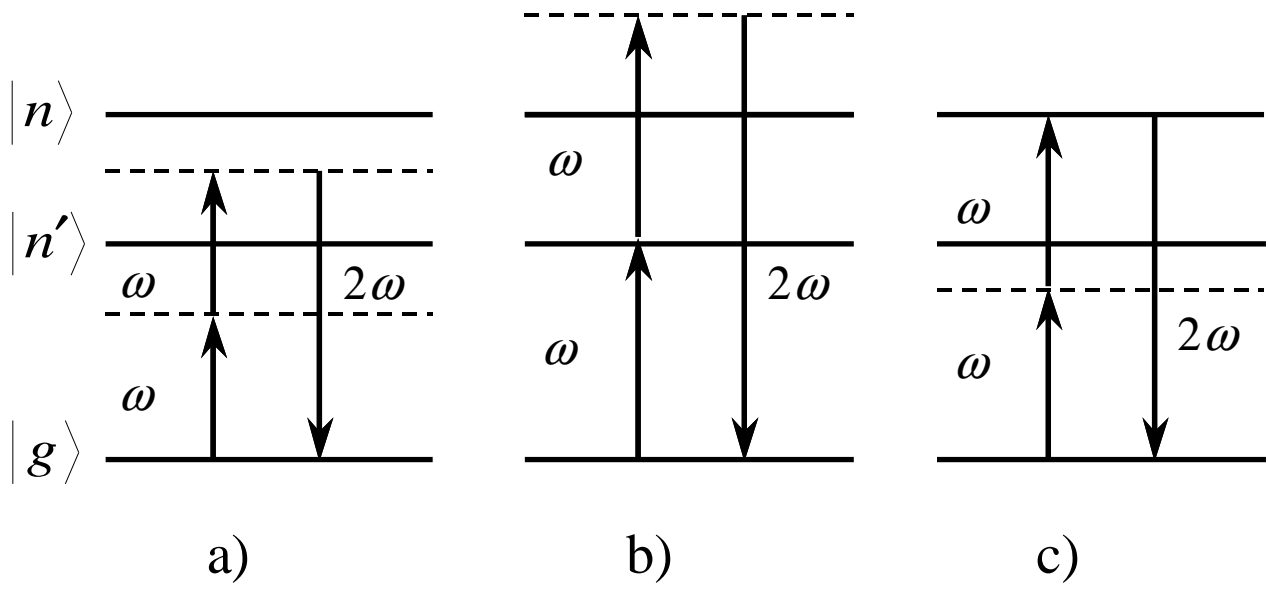


Fig. 4

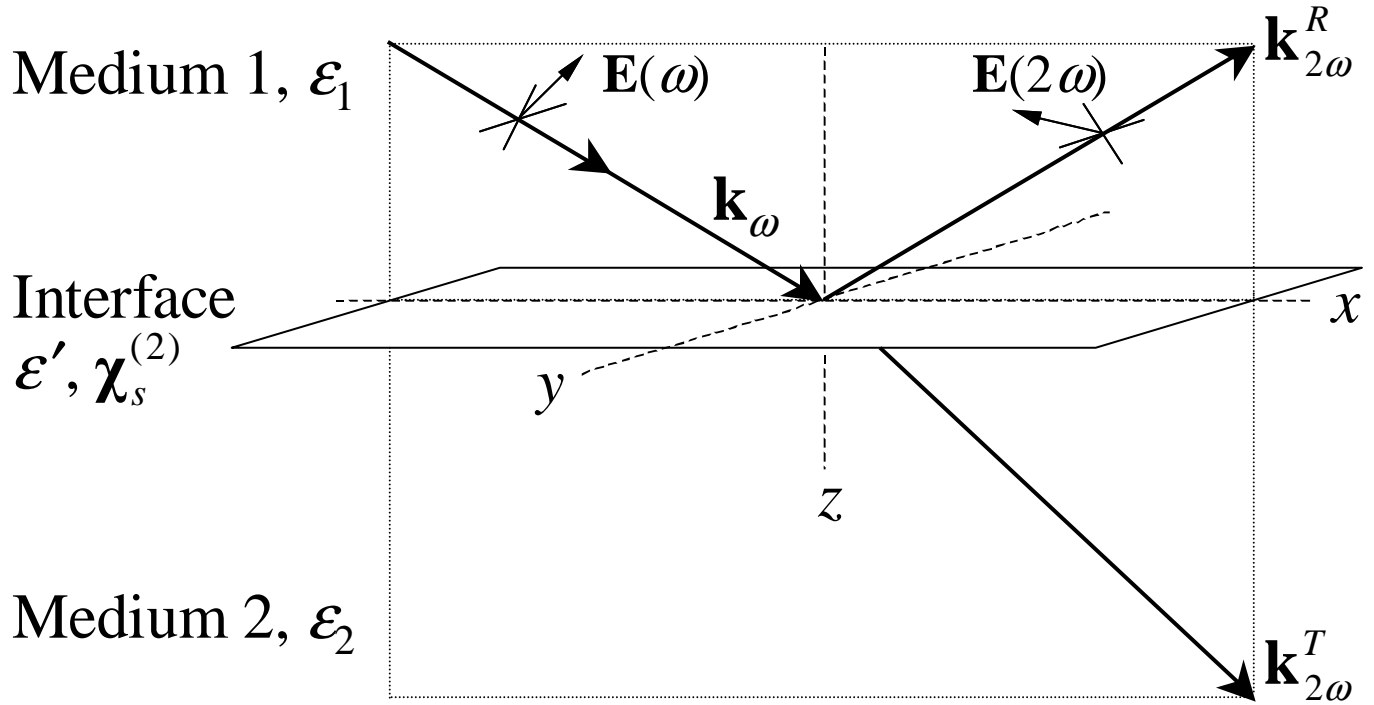


Fig. 5

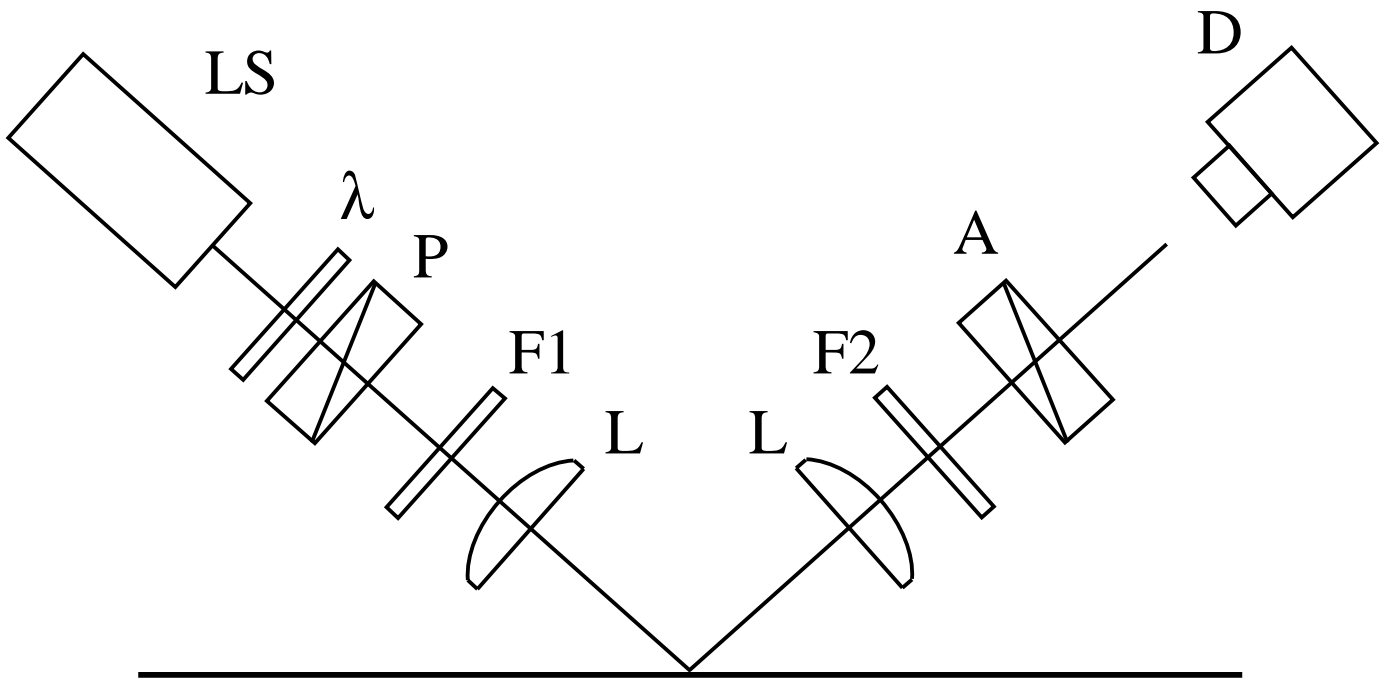


Fig. 6

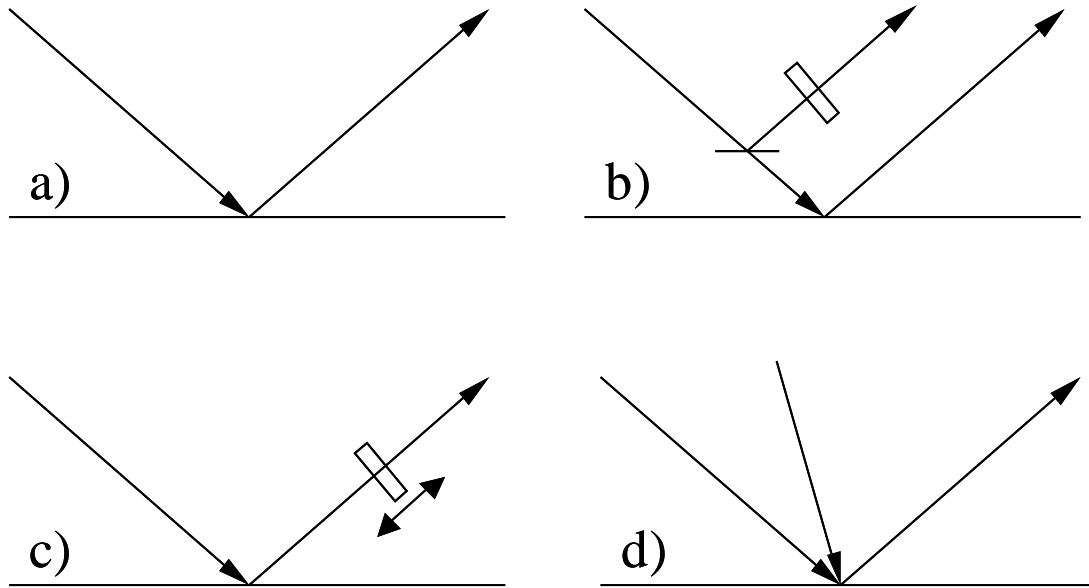


Fig. 7

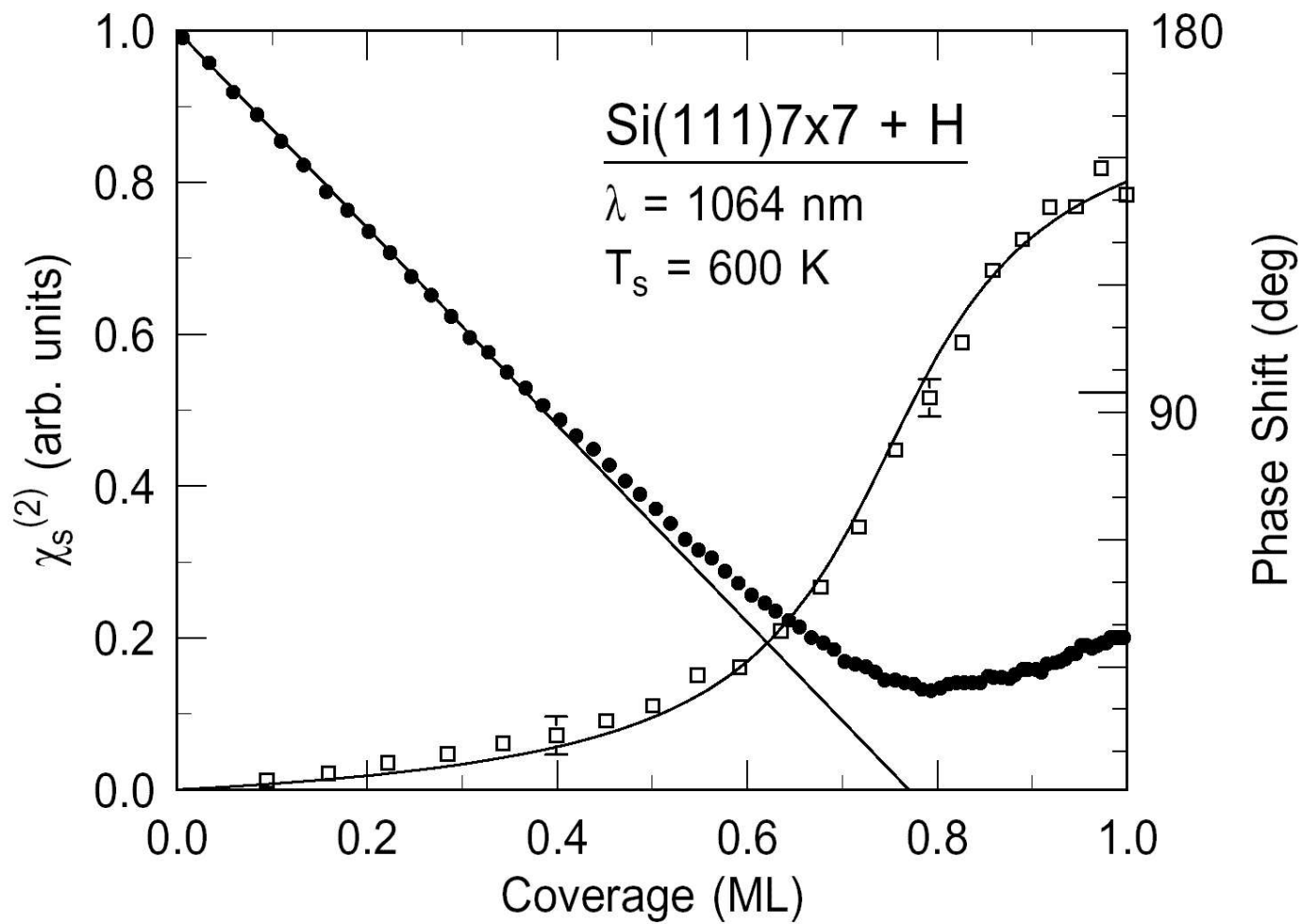
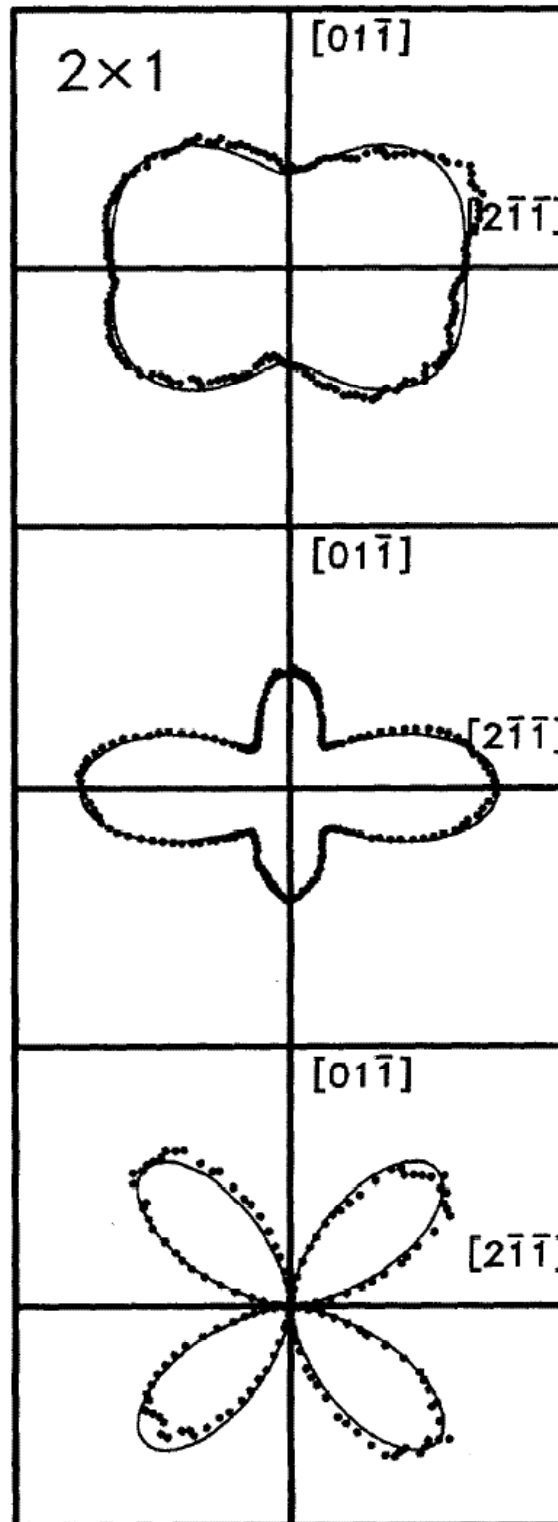


Fig. 8



(a)

Fig. 9

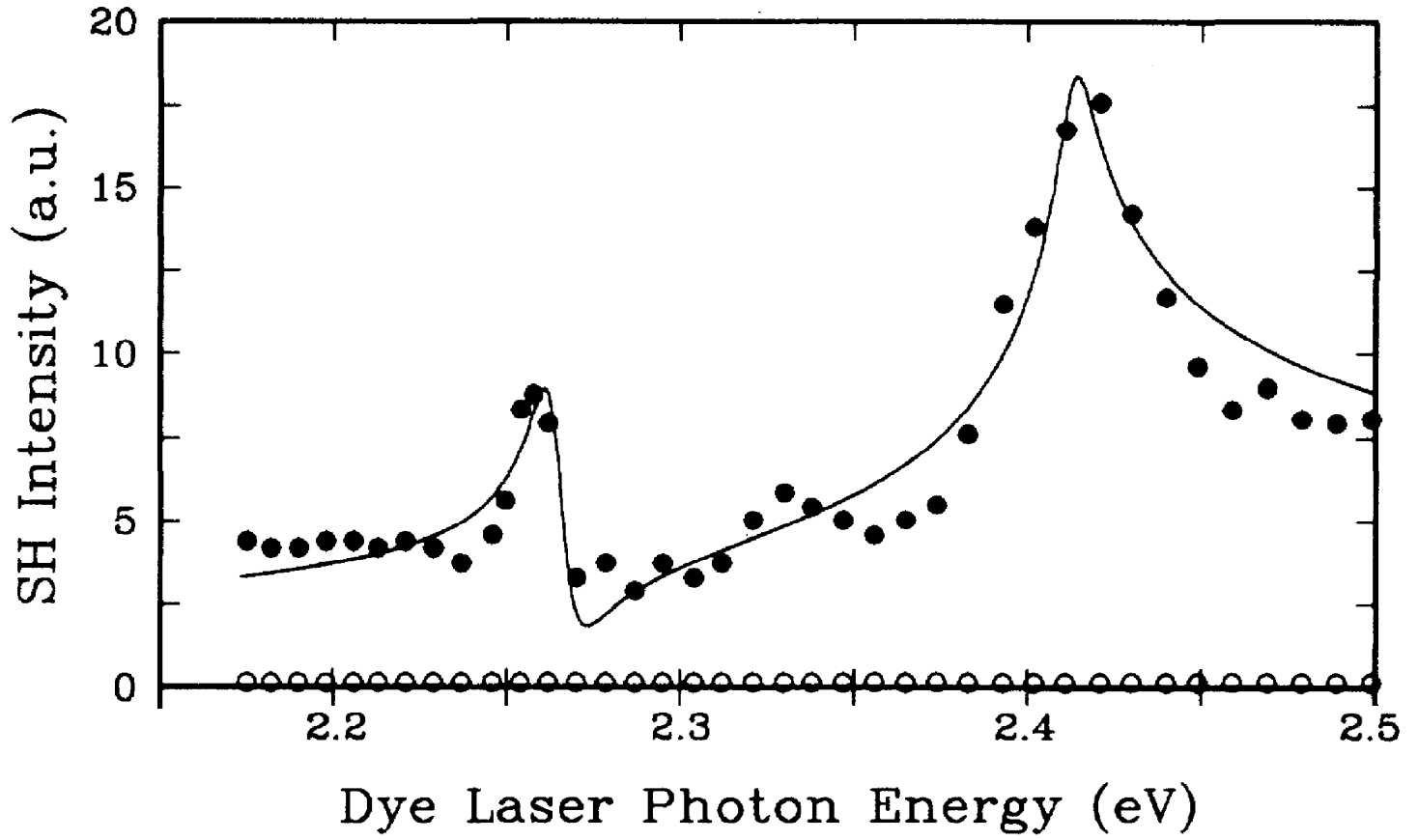


Fig. 10

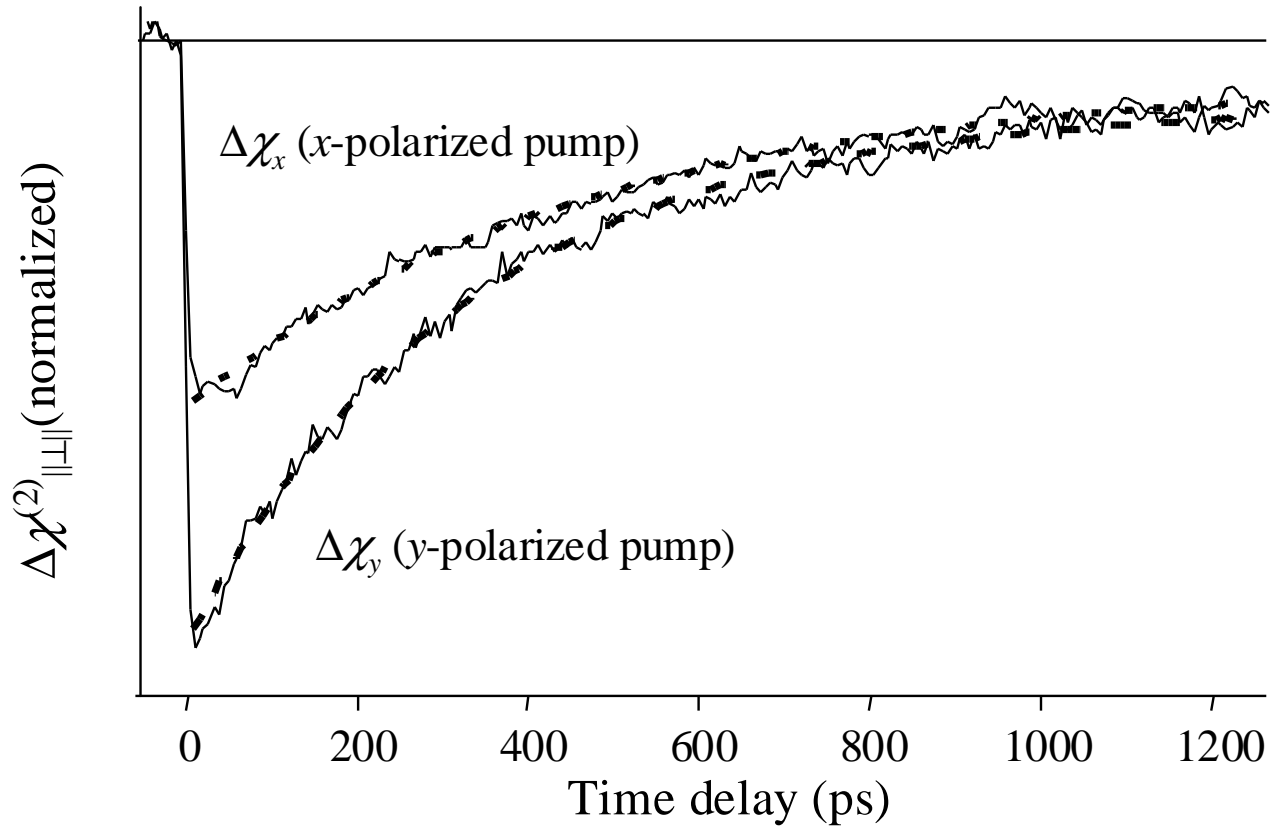


Fig. 11

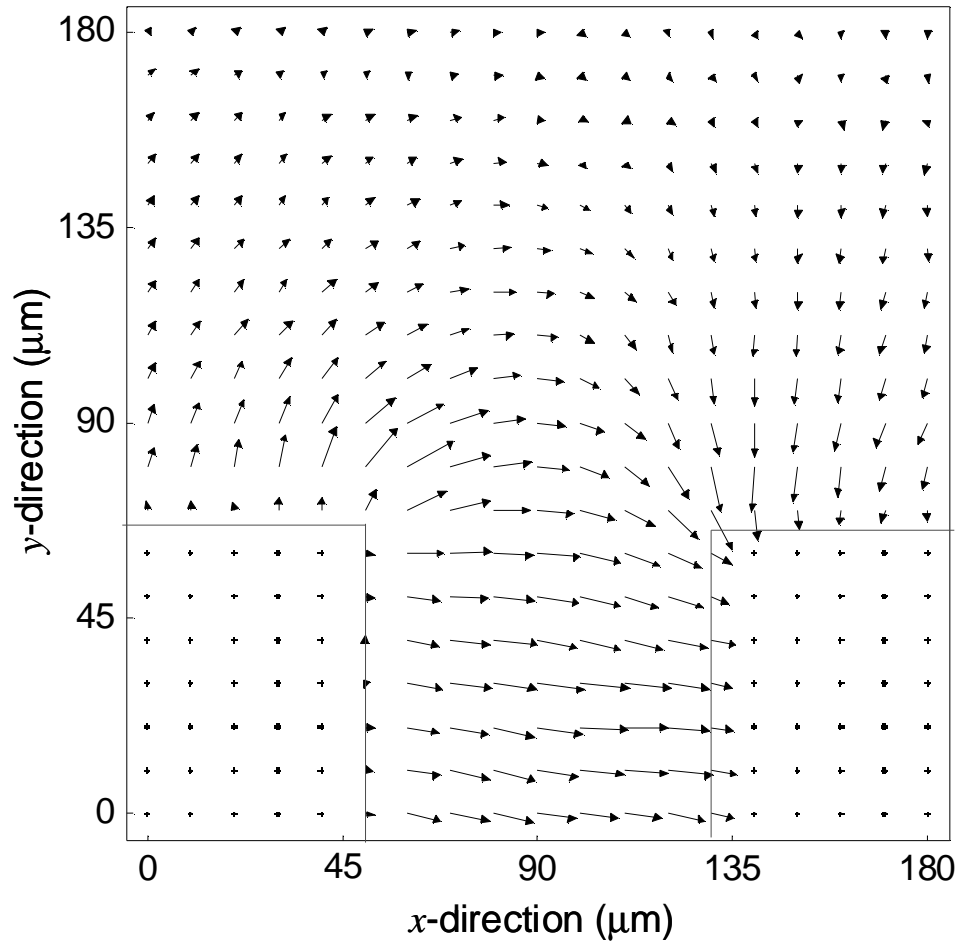
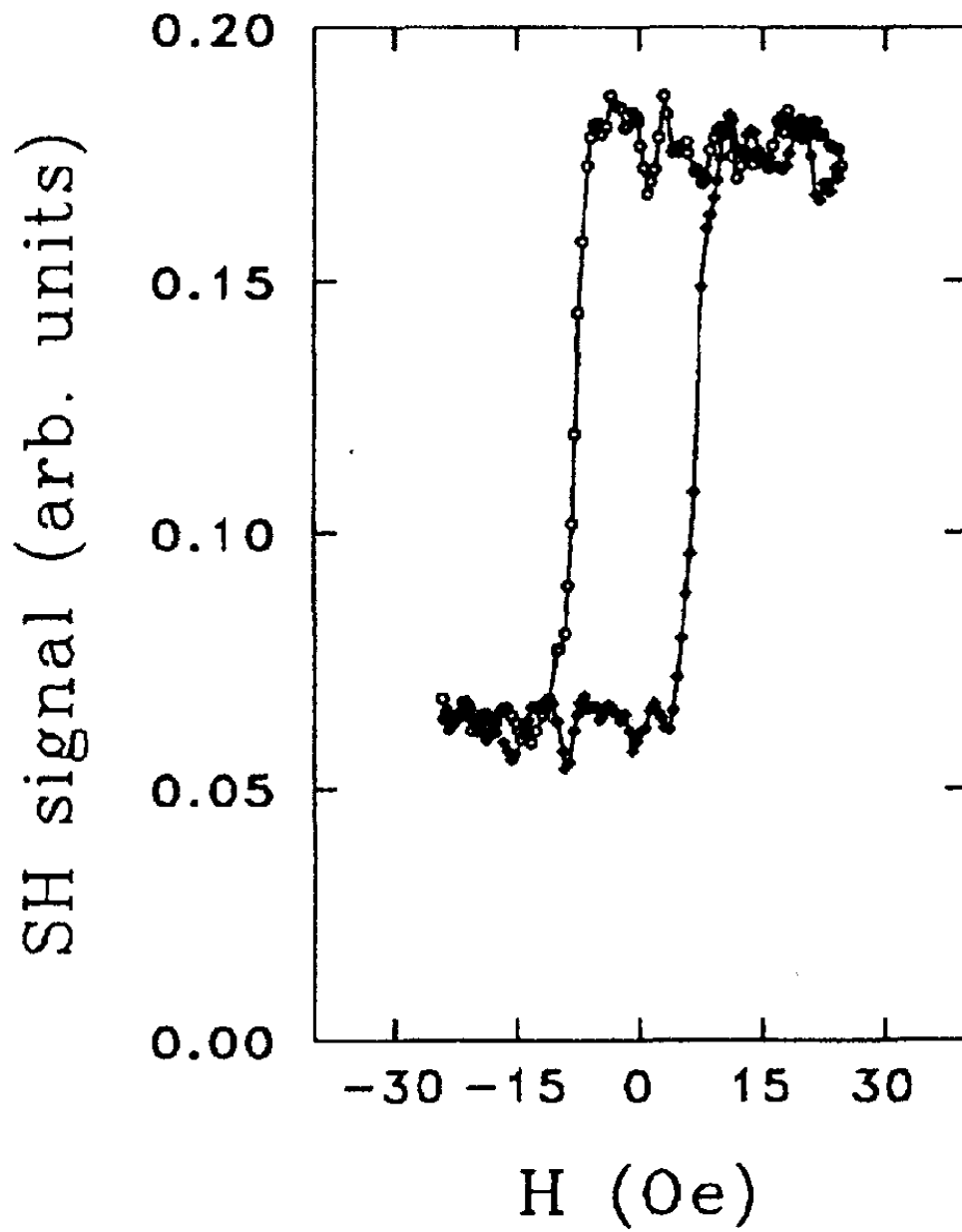


Fig. 12



REFERENCES

Books on surface second-harmonic generation

1. McGilp JF, Patterson CH, and Weaire DL eds. (1995) *Epioptics: linear and nonlinear optical spectroscopy of surfaces and interfaces*. Berlin; New York: Springer.
2. Brevet PF (1997) *Surface Second Harmonic Generation*. Lausanne: Presses Polytechniques et Universitaires Romandes.
3. Bennemann KH. ed. (1998) *Nonlinear Optics in Metals*. Oxford: Clarendon.

Books on nonlinear optics

1. Bloembergen N (1965) *Nonlinear optics*. New York: W.A. Benjamin.
2. Shen YR (1984) *The Principles of Nonlinear Optics*. New York: Wiley.
3. Butcher PN and Cotter D (1990) *The Elements of Nonlinear Optics*. Cambridge: Cambridge.
4. Prasad PN and Williams DJ (1991) *Introduction to Nonlinear Optical Effects in Molecules and Polymers*. New York: Wiley.
5. Boyd RW (1992) *Nonlinear Optics*. New York: Academic.

Selected reviews on surface nonlinear optics

1. Richmond GL, Robinson JM, and Shannon VL (1988) "Second harmonic generation studies of interfacial structure and dynamics," *Prog. Surf. Sci.*, 28, 1-70 .
2. Shen YR (1989) "Optical second harmonic-generation at interfaces," *Annu. Rev. Phys. Chem.*, 40, 327-350.
3. Heinz TF (1991) "Second-order nonlinear optical effects at surfaces and interfaces," *Nonlinear Surface Electromagnetic Phenomena*, Ponath H-E and Stegeman GI eds. Amsterdam: North Holland. pp. 353-416.
4. Corn RM and Higgins DA (1994) "Optical second-harmonic generation as a probe of surface-chemistry," *Chem. Rev.*, 94, 107-125.
5. Reider GA and Heinz TF (1995) "Second-order nonlinear optical effects at surfaces and interfaces: recent advances," *Photonic Probes of Surfaces*, Halevi P ed. Amsterdam: Elsevier pp. 413-478.
6. Liebsch A (1995) "Electronic excitations at metal surfaces," *Photonic Probes of Surfaces*, Halevi P ed. Amsterdam: Elsevier pp. 479-532.

7. McGilp JF (1995) "Optical characterisation of semiconductor surfaces and interfaces," *Prog. Surf. Sci.*, 49, 1-106.
8. Eisenthal KB (1996) "Liquid interfaces probed by second-harmonic and sum-frequency spectroscopy," *Chem. Rev.*, 96, 1343-1360.
9. Richmond GL (1997) "Vibrational spectroscopy of molecules at liquid/liquid interfaces," *Anal. Chem.*, 69, A536-A543.
10. Lüpke G (1999) "Characterization of semiconductor interfaces by second-harmonic generation," *Surf. Sci. Rep.*, 35, 75-161.
11. McGilp JF (1999) "Second-harmonic generation at semiconductor and metal surfaces," *Surf. Rev. Lett.*, 6, 529-558.
12. Dadap JI and Heinz TF (2001) "Nonlinear Optical Spectroscopy of Surfaces and Interfaces," *Encyclopedia of Chemical Physics and Physical Chemistry*, eds. Moore JH and Spencer ND Bristol: IOP, pp. 1089-1125.